MNK Publication

International Journal of Latest Research in Science and Technology **ISSN (Online):2278-5299**
Volume 3, Issue 2: Page No.80-89 ,March-April, 2014
https://www.mnkpublication.com/journal/ijlrst/index.php

NUMERICAL MODELING OF TRANSIENT THERMAL MIXING

[1]Murthy Lakshmiraju, [2]Jie Cui
[1]Graduate Student, Mechanical Engineering Department, Tennessee Technological University, Cookeville, TN, USA
[2]Professor, Mechanical Engineering Department, Tennessee Technological University, Cookeville, TN, USA

Abstract- In this paper, transient thermal mixing induced by a sudden transverse injection of a fluid into a main flow of different temperature was studied using the Reynolds Stress Model in the commercial computational fluid dynamics (CFD) software Fluent 6.4. The results obtained were validated with the existing experimental data. It was shown that the flow and temperature fields near the injection point were highly complicated and significant temperature fluctuations were observed in the mixing region. The results indicate that the mixing process depends on the momentum ratio of the main flow to the injection flow.

Keywords **-** Numerical Simulation, Transient thermal mixing, Sudden injection, Turbulence, Reynolds Stress Model

I. INTRODUCTION

The problem of transverse injection of a fluid into a confined cross-flow has many industrial applications, such as in nuclear safety analysis, air film cooling of gas turbine hot components, cooling of electronic components, mixing of two fluids in chemical industries, cooling water discharge systems for thermal power plants, etc. For example, in a Boiling Water Reactor of a nuclear power plant, reactor clean-up water is injected into the main feed water flow. In general, the clean-up water line is mounted transversely to the feed-water line. During the start-up and shut-down operations, the clean-up water was suddenly injected into the main flow. Typically, the main feed-water line and the injection flow are at different temperatures. The sudden transverse injection of a fluid in a moving stream produces a mixing region around and downstream of the injection point with high temperature gradients along radial, circumferential and longitudinal directions. This local temperature fluctuations cause significant thermal stresses on the surface of the pipe wall. These thermal stresses results in subsequent strain variations on the pipe wall resulting in fatigue damage and cracking of the pipes. It is a very important safety issue for the nuclear industry. Thus an understanding of the mixing phenomena is vital to estimate the effects of thermal stresses on the life of the pipe wall.

The thermal transients induced by a sudden transverse injection of a fluid into a main flow of different temperature have been studied both experimentally and numerically for decades. The mixing process depends on the combinations of flow rates, temperature differences, geometrical size, and thermo-physical properties of the main and injection flows [1].

Thermal mixing of a high pressure injection coolant that is injected into the cold leg of a pressurized water reactor was studied by many researchers. Schetz [1] have collected and reported mean-flow and turbulence data for the injection and mixing flow problems of general engineering interests. Hassan et al. [2] have studied the mixing process of a buoyant jet injected into a hot flow, numerically. It was found that for certain values of jet Froude numbers (ratio of inertial to buoyancy forces), hot water has ability to penetrate into the injector producing a strong recirculation region enhancing the mixing. Analytical model developed by Kim et al. [3] can be used for steady state flows with different injection angles, flow rate ratios and temperature ratios between the loop flow and the cold jet. A number of experimental studies have been reported on thermal mixing process. Moriya et al. [4] performed thermal transient water tests to study the effects of Reynolds number on thermal stratification using a simplified hot plenum model. It was found the rising speed of the interface and the temperature gradient at the interface were strongly related to the Reynolds number. Hafner et al. [5] observed an increase in the mixing with increase in the Froude number or by decreasing the nozzle diameter.

Konduri [6] and Khodabaksh et al. [7] investigated the transient thermal mixing induced by a sudden injection of a fluid into a main flow of different temperatures. Significant circumferential and axial temperature gradients were observed in the mixing region. It was also found that the high momentum of the combined flows excluded the possibility that buoyancy effects were significant in the initially stratified flows.

Wakamatsu et al. [8] studied the attenuation of temperature fluctuations in mixing jet streams impinging on the wall surface. It was observed that the surface attenuation ratio decreased with the jet flow velocity. Lele et al. [9] developed an analytical thermal hydraulic model based on lumped parameter model for predicting the Pressurized Thermal Shock in the down-comer in case of Emergency Coolant Injection. Hirota et al. [10] presented the experimental results on the turbulent mixing of hot and cold airflows in a T-junction with varying velocities and

Publication History
Manuscript Received : *26 April 2014*
Manuscript Accepted : *28 April 2014*
Revision Received : *29 April 2014*
Manuscript Published : *30 April 2014*

temperatures in an HVAC unit used for an automobile air conditioning system. It was observed that the mean temperature in the thermal mixing layer was uniform along the width, and the strong turbulence produced around the separation bubble does not work effectively to the thermal mixing of hot and cold airflows.

In recent years, thermal mixing and temperature fluctuations were studied using the available commercial CFD codes around a T-junction by Fukushima et al. [11], Metzner et al. [12], Chapuliot et al. [13], and Hu et al. [14]. Fukushima et al. [11] presented Direct Numerical Simulation and experimental results of turbulent thermal mixing in two square ducts connected via a T-junction. It was found that the temperature fluctuations on the walls were caused by various kinds of large-scale coherent structures near the T-junction. Hu et al. [14] carried out benchmark studies on a mixing tee configurations using Large Eddy simulation turbulence model. Simulations were performed for co-current and collision type mixing tee configurations.

In summary, many experimental, numerical and analytical analyses were performed on transient thermal mixing due to injection of a fluid into a main flow with different temperature. From the literature it was observed that the flow in the mixing region was highly turbulent and the wall temperature fluctuations are large. To the best knowledge of the authors, most of the researchers have performed studies on a steady mixing process and little work has been published on the transient mixing due to sudden transverse injection.

The main objective of this research is to study transient thermal mixing due to sudden transverse injection by performing numerical simulations with Reynolds Stress Model using commercial CFD software Fluent 6.4. The numerical model was set up based on the experiments performed by Khodabaksh et al. [7] and the results were validated with the experimental data. Furthermore, parametric studies were included to study the temperature fluctuations by varying main and the injection flow rates.

The present paper is organized as follows: the numerical method was presented in Section 2, validation of the numerical results against experimental measurements discussed in Section 3. Section 4 is concerned with the detailed analysis of the temperature fluctuations and Section 5 provides conclusions of this study.

II. NUMERICAL METHOD

Water was considered as the fluid at constant fluid properties and the values were shown in Table 1.

Table 1. Water properties used in the numerical simulations

Property	Values
Density	998.2 kg/m^3
Specific heat	4,182 J/kg-K
Thermal conductivity	0.6 W/ m-K
Viscosity	0.001 kg/ m-s

Flow was assumed to be incompressible and the buoyancy affects were not considered in the present numerical model. The mass conservation equation is:

$$\frac{\partial U_i}{\partial x_i} = 0 \quad (1)$$

where U_i are the Cartesian velocity component (i=1,2 and 3), x_i are the coordinate axes, and the repeated indices imply summation over 1 to 3. The Reynolds averaged momentum equations are defined as

$$\rho\left(\frac{\partial U_i}{\partial t} + \frac{\partial}{\partial x_j}(U_i U_j)\right) = -\frac{\partial P}{\partial x_i} + \frac{\partial}{\partial x_j}\left(\mu\left(\frac{\partial U_i}{\partial x_j} + \frac{\partial U_j}{\partial x_i}\right) - \rho\overline{u_j' u_i'}\right) \quad (2)$$

where P is the pressure, ρ is the density, μ is the dynamic viscosity, u_i' is the velocity fluctuation component, and $-\rho\overline{u_i' u_j'}$ is the averaged Reynolds stresses. As the flow near the mixing region was highly turbulent due to the presence of strong streamline curvatures, Reynolds Stress turbulence model was adopted since it has greater potential to provide the accurate predictions for these kinds of complex flows [15].

Reynolds Stress model was used to model the Reynolds stresses $\left(\tau_{ij} = \rho\overline{u_i' u_j'}\right)$, using individual transport equations together with an equation for the dissipation rate. The transport equations for the transport of the Reynolds stresses, τ_{ij} for an incompressible flow without body forces, are defined as

$$\frac{D\tau_{ij}}{Dt} = D_{T,ij} + D_{L,ij} + P_{ij} + \varphi_{ij} + \varepsilon_{ij} \quad (3)$$

where, $\frac{D\tau_{ij}}{Dt}$ is the total derivative of the Reynolds stresses, $D_{T,ij}$ is the turbulent diffusion, $D_{L,ij}$ is the molecular or viscous diffusion term, P_{ij} is the stress production term, φ_{ij} is the pressure-strain and ε_{ij} is the dissipation term. Of the various terms in Equation 3, $D_{L,ij}$ and P_{ij} do not require any modeling. However, $D_{T,ij}$, φ_{ij}, ε_{ij} need to be modeled to close the equations. A detailed description of the model can be found in [15] and Pope [16].

With the Reynolds stress model, turbulent heat transport is modeled using the concept of Reynolds' analogy to turbulent heat transfer. The modeled energy equation is given by

$$\frac{\partial}{\partial t}(\rho E) + \frac{\partial}{\partial x_i}[U_i(\rho E + P)] = \frac{\partial}{\partial x_j}\left[\left(k + \frac{C_p \mu_t}{Pr_t}\right)\frac{\partial T}{\partial x_j}\right] \quad (4)$$

where E is the total energy, C_p is the specific heat of fluid at constant pressure, T is the temperature. The turbulent Prandtl number is 0.85.

In the present study, for near wall modeling, enhanced wall treatment was used to bridge the viscosity affected region between the wall and the fully turbulent region. The coupling between the velocity field and pressure field is strong for incompressible flows. The SIMPLE algorithm was employed to relate velocity and pressure corrections to enforce mass conservation and to obtain the pressure field. A second order upwind scheme was used to avoid numerical oscillations and instability associated with central differencing for convective terms in the transport equation and to increase the accuracy of solutions [15].

III.NUMERICAL SIMULATION

3.1 Simulation Setup

Fluent uses Gambit as an integrated preprocessor, for geometry construction and mesh generation. Numerical model was developed based on the experimental setup of [7].

Main feed water line and the injection line was numerically modeled and is shown in Figure 1. The inner diameters of the main feed water line and the injection lines were 6.1 in (0.155m) and 1.6 in (0.04m). The injection line was radially into the feed water line at an angle of 45^o to the horizontal. The dimensions of the model were also presented in Figure 1.

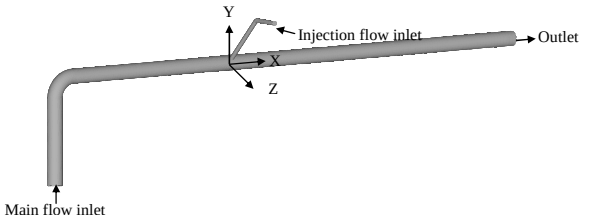

(a) Isometric view

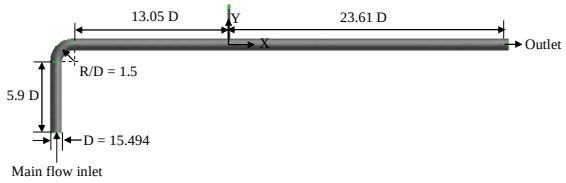

(b) XY view

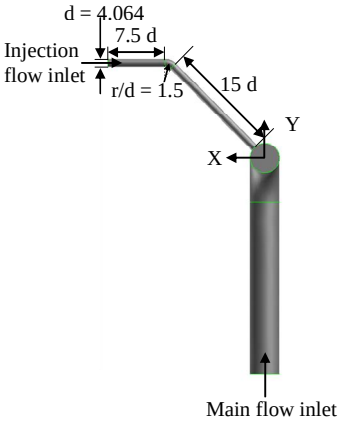

(c) YZ view

Fig. 1 Numerical model (a) isometric (b) XY and (c) YZ views (Dimensions are in cm).

In order to avoid the stability and convergence difficulties, a structured grid using hexahedral elements was generated in the fluid domain. The geometry was subdivided into 74 volumes in order to generate a structured mesh. As the temperature fluctuations in the near-wall region are of primary concern, it is ensured that the first computational grids are fine enough to resolve the viscous sub-layer. In the current study, the first grid center was located at a value of two wall units from the wall and this ensures in resolving the viscous sub layer. The velocity and temperature gradients were high near injection point; mesh was also refined in these regions to get better resolution. A refined structured mesh at the mixing region was shown in Figure 2(a). Figure 2(b) shows the structured mesh at any given cross section of the main pipe with refined mesh near the walls. The total number of mesh elements was around 928,000.

To validate the numerical model the boundary conditions were considered same as those presented in Khodabaksh et al. [7]. To model the sudden injection of fluid into the main feed water line, initially flow has to be modeled only in the main feed water line and after establishing a steady flow then fluid was injected radially at an angle of 45^o into the main feed water line through the injection pipe. After reaching the steady state in the main line, the transient process was enabled with a gradual increase of the injection flow rate over a 20 second time period to consider the time taken for opening the injection flow valve, starting the injection pump and reaching the full capacity (i.e. a soft start). This gradual increase in the injection flow rate was specified using a User Defined Function (UDF) at the injection inlet.

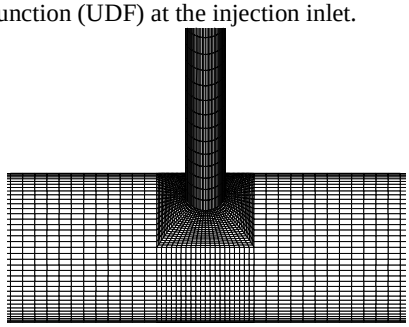

(a) Near the injection region

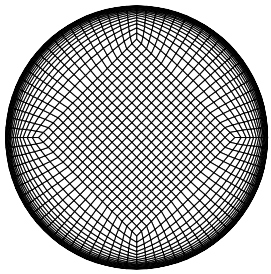

(b) At the cross-section of the main pipe

Fig. 2 Structured mesh (a) near the injection region (b) at the cross-section of the main pipe.

Khodabaksh et al. [7] presented detailed results for a case with flow rates of 1.694 kg/s at 298.5 K (77^o F) at main feed water line and 5.4 kg/s at 366.5 K (200^o F) at the injection line. At these flow rates, the average velocities in the main pipe (diameter, D = 15.494 cm) and injection pipes (diameter, d = 4.064 cm) were 0.09 m/s and 4.17 m/s, respectively. The ratio of average velocity of the injection pipe to the main pipe was around 46.3. In the numerical model, these mass flow rates of 1.694 Kg/s (Re ≈ 14,000) and 5.4 Kg/s (Re ≈ 170,000) were imposed at the main flow inlet and the injection inlet respectively. On the walls, no slip boundary condition was applied. As the pipe walls were not insulated in the experiments, a heat transfer coefficient of 50 W/m^2.K was imposed on the walls of the numerical domain. A zero Pascal relative static pressure with a back flow total temperature of 298.5 K (77^o F) was imposed at the exit of the main feed water line.

Depending on the momentum ratio of the main flow to the injection flow, the mixing pattern is divided into wall

jet, deflecting jet, and impinging jet. The momentum ratio is defined as [14]:

$$M_R = \frac{\rho_m V_m^2 D_m^2}{\rho_i V_i^2 D_i^2} \quad (5)$$

where M_R is the momentum ratio, V is the velocity, D is the diameter, and subscript m and i denote the parameters for main and injection pipes, respectively. A flow pattern is said to be an impinging jet if the momentum ratio is less than 0.35, a wall jet if the ratio is greater than 1.35 and a deflecting jet if the ratio is between 0.35 and 1.35. A jet is defined as an impinging jet when the injection jet impinges on the bottom of the main pipe wall, wall jet- when the injection jet does not reach the center axis of the main pipe and deflecting jet when the jet has an intermediate characteristics of the two jets mentioned above.

In addition to the baseline case two parametric studies were also performed by varying main and injection flow rates to study the effects of the main and the injection flow rates on the temperature fluctuations. Varying main flow and injection flow rate studies were performed by halving and doubling the respective flow rates. Each parametric study was performed without changing the other boundary conditions. The mass flow rates and temperatures for various cases were shown in Table 2.

Table 2. The mass flow rates and temperatures at main and injection flows for various cases

	Main flow		Injection flow	
	Mass flow rate (Kg/s)	Temperature (K)	Mass flow rate(Kg/s)	Temperature (K)
Base line	1.693	298.5	5.4	366.5
Half main flow rate	0.846	298.5	5.4	366.5
Double main flow rate	3.387	298.5	5.4	366.5
Half injection flow rate	1.69	298.5	2.7	366.5
Double injection flow rate	1.69	298.5	10.8	366.5

For initial steady flow in the main feed water line, calculations were started with standard k-ε turbulence model and the k-ε data was used as a starting point for the Reynolds stress model calculations. For both the standard k-ε and Reynolds stress turbulence models, convergence was claimed when the residuals were found to reduce by four orders of magnitude. In order to confirm the convergence, velocities were monitored at different locations close to the injection region. After obtaining the steady state solution for the main feed water line, transient solver was enabled with the injection flow. For transient formulation, second order implicit scheme was used with a fixed iterative time advancement scheme. A step size of 0.2 seconds and 20 iterations per time step was considered and the simulations were performed for a total of 100 seconds. Numerical simulations were performed on a Dell Precision Workstation 690n with 2 Intel Xeon 5365 Processors (3.0 GHz, 2 x 4MB L2 cache, 1333 FSB), 32GB SDRAM FBD, ECC with 667 MHz and 2 x 300GB 10K rpm SAS hard drives. A typical steady simulation took approximately 9 hrs and transient simulations took around 16 hrs.

3.2 Code Validation

Khodabaksh et al. [7] monitored wall temperatures at several locations in the downstream of the test section by means of thermocouples mounted flush with the wall. Temperatures were monitored at a total of five axial locations from the injection point as shown in Figure 3(a). At each of the first four stations, six thermocouples were placed around the circumference at even increments from the injection point and at the last station; four thermocouples were installed at even increments. The circumferential locations of the thermocouples were shown in Figure 3(b). Temperatures were monitored at 28 different locations to understand the temperature variations in the experimental test section. The wall temperatures were recorded using a data-logger for every two seconds.

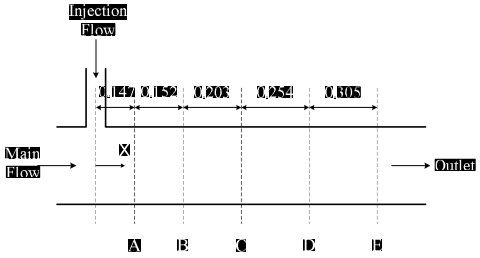

(a) Along the axial direction (units in meters)

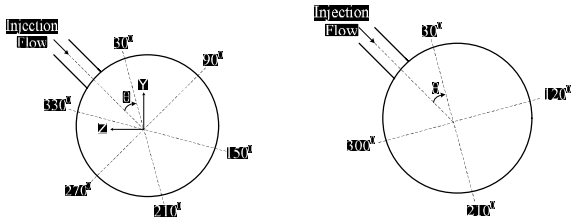

Stations: A, B, C and D Station E

(b) Along the circumferential direction

Fig. 3 Thermocouple locations in the test section (a) along the axial direction (b) along the circumferential direction (not to scale).

To compare with the experimental results temperatures in numerical calculations were monitored with respect to time at all 28 locations that are mentioned above. Temperature profiles at Station A and Station C measured at an angle of 150^o from the injection point were presented in Figures 4(a)

and 4(b) respectively. From both the figures it can be observed that numerical simulations with 928,000 elements and time step size 0.2 seconds were in good agreement with the experimental results. A detailed discussion on the transient temperature profiles were presented in Section 4: Results and Discussions.

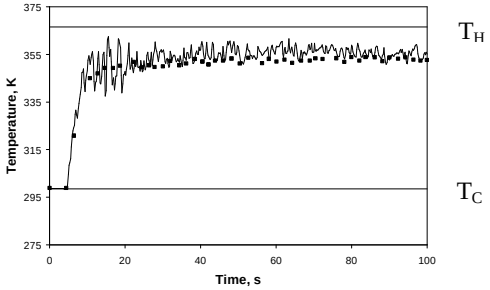

(a) Station A and 150^o from the injection point

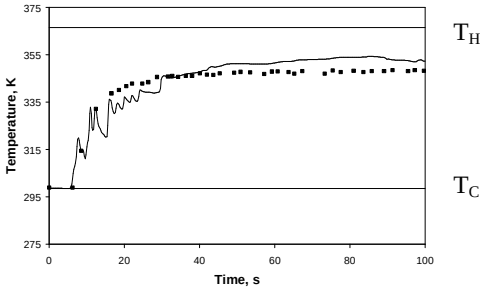

(b) Station C and 150^o from the injection point

Fig. 4 Comparison of the temperature profiles of experimental and numerical results at (a) Station A and 150^o from the injection point and (b) Station C and 150^o from the injection point (Symbols – Experimental results by Khodabaksh et al. [7] and solid line – numerical results with 928,000 elements with a time-step of 0.2 seconds).

IV. THE RESULTS AND DISCUSSIONS

4.1 Baseline case

For the baseline case, the momentum ratio is 0.0067 and the value is less than 0.35 therefore the injection jet can be assumed as an impinging jet. Figure 4 shows the temperature profiles after injection of hot water into the main flow at Station A and Station C measured at an angle of 150° from the injection point. At all the stations the temperature profiles were similar. The wall temperatures were same as that of the main flow temperature until the hot injection jet impinges on the wall and then a sharp rise in the temperature was observed. The rise in the temperature can be observed at Station A and Station C at flow time steps of 4.0 seconds and 6.2 seconds respectively after the injection flow starts. The temperature rise by 56.5 K was observed within 5.6 seconds after the first initial temperature rise. After the mixing of the hot and cold flows, temperature of the water settled down at nearly 354.2 K and 351 K at Station A and Station C respectively. Higher temperature was observed at Station A when compared to other stations. As Station A was closer to the injection point, this station was subjected to continuous hot and cold flows, therefore high temperature fluctuations were observed when compared to other stations in the downstream of the injection point. It can also be observed that the thermal response was slower at Station C when compared to Station A. From the figure, it can be concluded that the numerical method successfully captured this transient process and the numerical results were in good agreement with the experimental data.

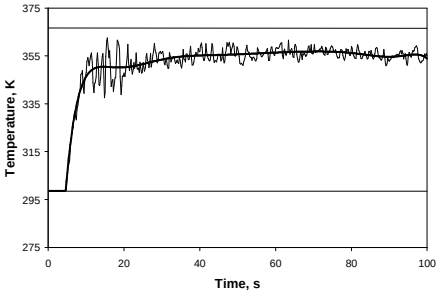

(a) Transient temperature profile with the polynomial curve fit

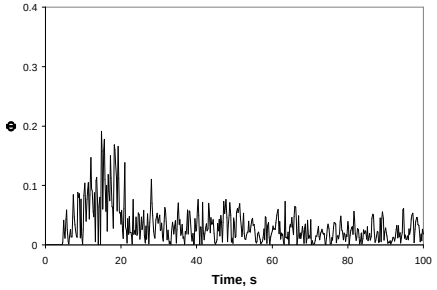

(b) Transient temperature fluctuations

Fig. 5 Transient temperature profile with the polynomial curve fit and the temperature fluctuations Station A and 150^o from the injection point (Thick line indicates the polynomial curve fit).

For Unsteady RANS (URANS) modeling, the temperature fluctuations can be calculated though ensemble averaging. Alternatively, a polynomial curve with an order of 10 was curve fitted for the transient temperature profile data for all the 28 locations that are mentioned in the previous section. Figure 5(a) and 6(a), presents the transient temperature profile and the polynomial fit at Station A and Station C measured at an angle of 150o from the injection point. Fluctuation temperature was calculated and normalized as shown in the following equation:

$$\Phi = \frac{T - T_{PF}}{T_H - T_C} \quad (6)$$

where T is the local temperature, TPF is the temperature from the polynomial curve fit, TH and TC are the temperatures for the baseline case of the injection flow (366.5 K) and the main flow (298.5 K), respectively. Figure 5(b) and 6(b) shows the normalized temperature fluctuations plotted at Station A and Station C measured at an angle of 150° from the injection point. Comparing the temperature fluctuations shown in Figure 5 with those in Figure 6 clearly indicates a dramatic change in the magnitude of the temperature fluctuations. In both the cases, the temperature fluctuations were initially zero and as the injection flow enters the main stream, high magnitude temperature fluctuations were observed at Station A when compared to that of Station C. At Station A, the highest normalized temperature fluctuation

was around 0.2 in 0.2 seconds (i.e. 13.6 K in 0.2 seconds) and at Station C, the highest normalized temperature fluctuation was 0.15 in 0.6 seconds (i.e. 10.2 K in 0.8 seconds). The initial increase in the fluctuations is due to the change in the injection flow rate for the first 20 seconds. After 20 seconds, the normalized temperature fluctuations magnitude (0 to 0.075) was higher at Station A 150° from the injection point when compared to the magnitude of the temperature fluctuations (0 to 0.01) at Station C 150° from the injection point. High temperature fluctuations were observed at Station A when compared to other stations as it was close to the injection point, where the hot and cold flows encounter, whereas in the downstream stations, the hot and cold fluids are gradually mixed and result in lower temperature fluctuations. These high temperature fluctuations near the injection point lead to the thermal stresses and strains on the pipe walls.

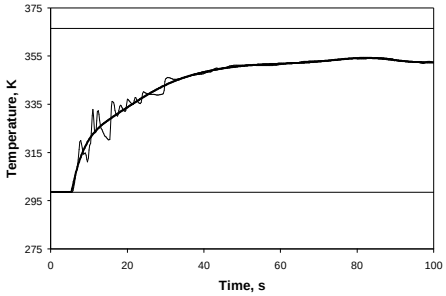

(a) Transient temperature profile with the polynomial curve fit

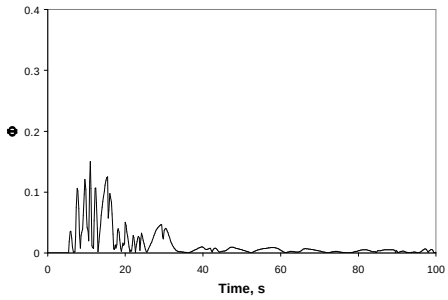

(b) Transient temperature fluctuations

Fig. 6 Transient temperature profile with the polynomial curve fit and the temperature fluctuations Station C and 150^o from the injection point (Thick line indicates the polynomial curve fit).

Figure 7 shows the normalized wall temperature profiles along the normalized axial direction at 0°, 90°, 180°, and 270° from the injection point at flow times of 20, 40, 60 and 80 seconds. Solid line, long dash line, dash dot dot line and dot line indicates the normalized temperatures at 0°, 90°, 180°, and 270° from the injection point, respectively. Figure 7 shows the temperature variation along the axial direction for a given time and temperature variation along the circumferential direction at a given X/D location for a particular time, where X is the axial location measured from the injection point and D is the diameter of the main pipe. Injection point was represented by 0D, upstream axial locations were represented by a negative sign and downstream locations were represented by positive signs. Normalized temperature was defined as shown in the following equation:

$$\Theta = \frac{T - T_C}{T_H - T_C} \quad (7)$$

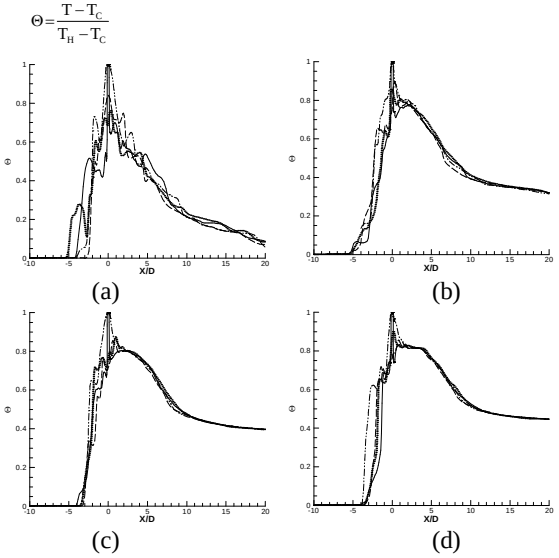

(a) (b) (c) (d)

Fig. 7 Comparison of the transient temperature profiles along the axial direction at 0^o, 90^o, 180^o, 270^o from the injection point at flow times of (a) 20 seconds, (b) 40 seconds, (c) 60 seconds and (d) 80 seconds (Solid line – 0^o, long dashed line – 90^o, dash dot dot line – 180^o, and dotted line – 270^o).

Figure 7(a) shows the axial and circumferential temperature variation at a flow time of 20 seconds. Between 0D to -5D, a drop in the normalized temperature of about 1 (68 K difference) was observed along the axis at 0° and 180° from the injection point. A normalized temperature drop of 0.8 (54.4 K difference) was observed along the 90° and 270° from the injection point between 0D and -3D. A sudden temperature drop of about 0.5 (34 K difference) was also observed around -2D within a span of 0.5D axial distance. A drop in the temperature was observed in the downstream but not as steep as in the upstream of the injection point. As expected, the maximum temperature variation was observed along the 180o from the injection point due to the high injection jet momentum when compared to that of the main flow momentum. From Figure 7(a), a maximum normalized temperature variation of about 0.5 (34 K difference) was observed along the circumferences at +0.5D and -0.5D axial locations. Circumferential temperature variations were observed between -5D and 20D at a flow time of 20 seconds. These sudden changes in the temperature gradient along the axial and circumferential directions increases the thermal stresses in the mixing region.

From Figures 7 (b), (c) and (d), it can be observed that the temperature variations were high along the axis in the upstream of the injection location between 0D and -4D. Similarly, high temperature variations were also observed in the upstream of the injection location between 0D and -4D along the circumference of a given axial location. The temperature variations were observed in the downstream of the injection point between 0D and 2D at different flow times but the temperature variations were not as high as that of in the upstream of the injection point. After an axial location of 2D, the axial temperature variations were decreasing with increase in the flow time. It can be observed that the maximum circumferential temperature variations were

observed close to the injection point both in the upstream and downstream of the injection point of about 0.4 (27.2 K difference) and 0.3 (20 K difference) respectively. After an axial location of 2D, the circumferential temperature variations were decreasing with respect to time and were almost negligible around 80 seconds flow time.

Figure 8 shows the stream line traces on the injection plane for flow times of 20 seconds, 40 seconds, 60 seconds and 80 seconds. From this figure it can be observed that the hot injection jet was entering into the main cold flow at an axial location of 0D. After the injection jet impingement on the bottom wall of the injection plane, the injection flow moves parallel to the wall in both upstream and downstream of the injection point. From the streamlines, it can be clearly seen that flow was highly turbulent and the swirling motion continuously changes its location shape and strength with change in the flow time. This was due to the interaction of the hot injection flow trying to move in the upstream of the injection point after the impingement and the cold main flow trying to move to the downstream. The effect of the injection flow was observed in both the upstream and the downstream of the injection point. Recirculation regions were observed in the upstream of the injection point due to the sudden injection of hot water into the main flow. Due to the entering of the high speed flow from the injection line, flow entrainment into the hot injection jet can be observed near the injection point in both the upstream and downstream locations. As the flow time increases the cold main flow responds to the injection flow therefore the number of recirculation region decreases and smooth cold flow streamlines were observed in the upstream far from the injection point.

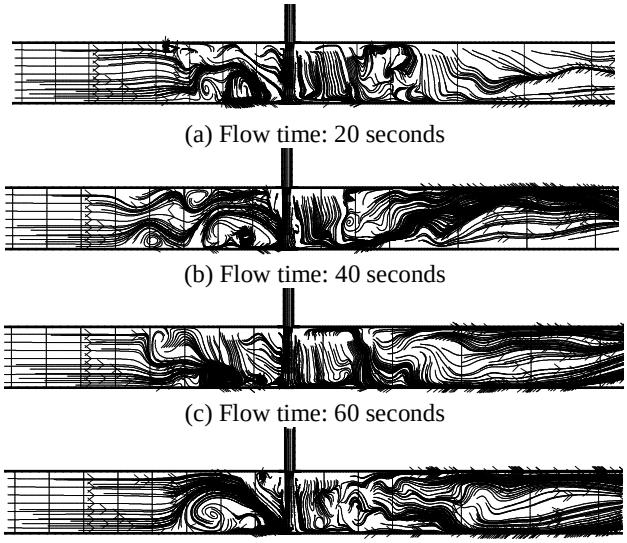

(a) Flow time: 20 seconds

(b) Flow time: 40 seconds

(c) Flow time: 60 seconds

(d) Flow time: 80 seconds

Fig. 8 Stream lines for the baseline case on the injection plane at for flow times of (a) 20 seconds, (c) 40 seconds, (d) 60 seconds and (e) 80 seconds

4.2 Varying main flow rate

In this parametric study, two cases were studied with halved and doubled main flow rates without changing the other boundary conditions. For halved and doubled main flow rate cases, the momentum ratios are 0.002 and 0.027. For both the cases, the momentum ratios are less than 0.35 and the injection jet can be considered as an impinging jet.

Figure 9 shows the transient temperature profiles for the varying main flow rate cases after injection of hot water into the main flow at Station A and Station C measured at an angle of 150o from the injection point. The temperature profiles were similar to that of a base line case. The wall temperatures were same as that of the main flow temperature until the hot injection jet mixes with the main flow and then a rise in the temperature was observed. For the half main flow rate, the rise in the temperature can be observed at Station A and Station C at flow time steps of 4.0 seconds and 6.2 seconds respectively after the injection flow starts. For the double main flow rate, the rise in the temperature can be observed at Station A and Station C at flow time steps of 4.9 seconds and 6.2 seconds respectively. Similar to the baseline case, higher temperatures were observed at Station A when compared to other stations.

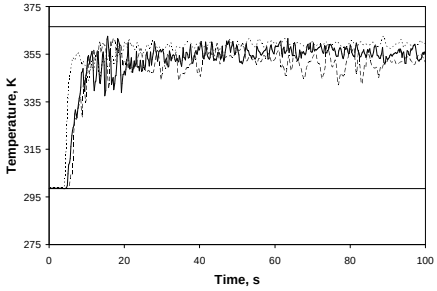

(a) Station A and 150^{o} from the injection point

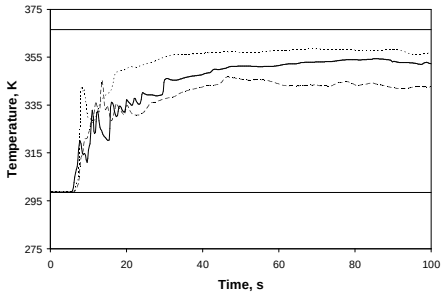

(b) Station C and 150^{o} from the injection point

Fig. 9 Comparison of the temperature profiles of varying main flow rates (a) Station A and 150^{o} from the injection point and (b) Station C and 150^{o} from the injection point (- solid line – baseline case, long dashed line – double main flow rate and short dashed line – half main flow rate).

From Figure 9, it can be observed that with increasing the main flow rate a decrease in the slope of the temperature rise was observed. For the half main flow rate case, the temperature rise by 57 K was observed within 3.8 seconds after the first initial temperature rise. Whereas for the double main flow rate case, the temperature rise by 57 K was observed within 8 seconds after the first initial temperature rise. When compared to the baseline case and double main flow rate case, the injection flow momentum was higher for the half main flow rate case and hence a quick increase in the temperature rise was observed. For the half main flow rate case, the temperature settled down at nearly 359.3 K and 357.7 K at Station A and Station C respectively. For the

double main flow rate case, the temperature settled down at nearly 351.8 K and 343.8 K at Station A and Station C respectively.

Similar to the baseline case, transient normalized temperature fluctuations were studied for the varying main flow cases by fitting a polynomial curves for the transient temperature profiles that were presented in Figure 9. Figures 10(a) and 10(b) shows the temperature fluctuations at Station A and Station C measured at an angle of 150° from the injection point for the half main flow rate case. Temperature fluctuations at Station A were higher than that of the fluctuations at Station C except for the initial temperature rise. At Station A, the highest normalized temperature fluctuation was 0.23 in 0.2 seconds (i.e. 15.6 K in 0.2 seconds) and at Station C, the highest normalized temperature fluctuation was 0.3 in 0.8 seconds (i.e. 20.4 K in 0.8 seconds). After 20 seconds, the temperature fluctuations magnitude was higher at Station A 150° from the injection point (0 to 0.06) when compared to the magnitude of the temperature fluctuations at Station C 150° from the injection point (0 to 0.01).

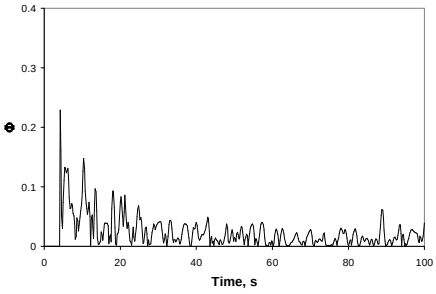

(a) Transient temperature fluctuations at A and 150^o

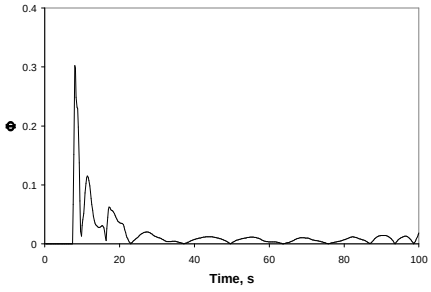

(b) Transient temperature fluctuations at C and 150^o

Fig. 10 Transient temperature fluctuations at Station A and Station C at 150^o from the injection point for the half main flow rate case.

Figures 11(a) and 11(b) shows the temperature fluctuations at Station A and Station C measured at an angle of 150o from the injection point for the double main flow rate case. The temperature fluctuations were similar to that of the fluctuations for the baseline case. At Station A, the highest normalized temperature fluctuation was 0.2 in 0.8 seconds (i.e. 13.6 K in 0.8 seconds) and at Station C, the highest normalized temperature fluctuation was 0.16 in 0.6 seconds (i.e. 10.8 K in 0.6 seconds). After 20 seconds, the temperature fluctuations magnitude was higher at Station A 150o from the injection point (0 to 0.13) when compared to the magnitude of the temperature fluctuations at Station C 150o from the injection point (0 to 0.02). Though with increased main flow rate the jet behaves as an impinging jet and the main flow momentum is comparably higher than the other two cases. Therefore, high temperature fluctuations were observed when compared to the baseline and half main flow rate cases. Hence, higher thermal stresses can be expected for the double main flow rate case when compared to the other cases.

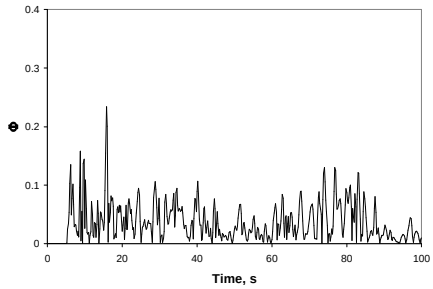

(a) Transient temperature fluctuations at A and 150^o

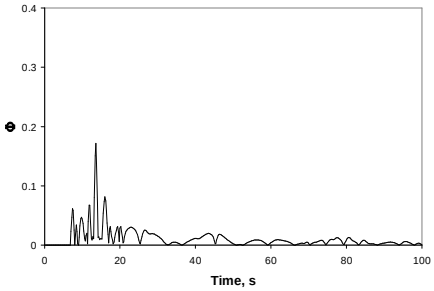

(b) Transient temperature fluctuations at C and 150^o

Fig. 11 Transient temperature fluctuations at Station A and Station C at 150^o from the injection point for the double main flow rate case.

4.3 Varying injection flow rate

In this parametric study, two cases were studied with halved and doubled injection flow rates without changing the other boundary conditions. For halved and doubled injection flow rate cases, the momentum ratios are 0.027 and 0.002. For both the cases, the momentum ratios are less than 0.35 and the injection jet can be considered as an impinging jet.

Figure 12 shows the transient temperature profiles for the varying injection flow rate cases after injection of hot water into the main flow at Station A and Station C measured at an angle of 150° from the injection point. The temperature profiles were similar to that of a base line case. With the increased injection flow rate, the initial temperature rise was quicker at all the stations. For the half injection flow rate, the rise in the temperature can be observed at Station A and Station C at flow time steps of 6.4 seconds and 8.6 seconds respectively after the injection flow starts. For the double injection flow rate, the rise in the temperature can be observed at Station A and Station C at flow time steps of 3.2 seconds and 4.4 seconds respectively.

From Figure 12, it can be observed that with increasing the injection flow rate an increase in the slope of the temperature rise was observed at both the stations. For the half injection flow rate case, the temperature rise by 46.5 K was observed within 3.6 seconds after the first initial temperature rise. Whereas a sudden temperature rise was

observed for the double injection flow rate case by 54.5 K within 3.1 seconds after the first initial temperature rise. For the half injection flow rate case, the temperature settled down at nearly 351.1 K and 342.4 K at Station A and Station C respectively. For the double injection flow rate case, the temperature settled down at nearly 359.2 K and 358.1 K at Station A and Station C respectively.

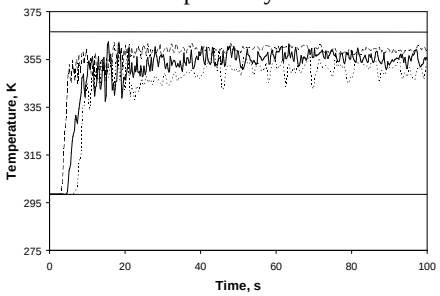

(a) Station A and 150^o from the injection point

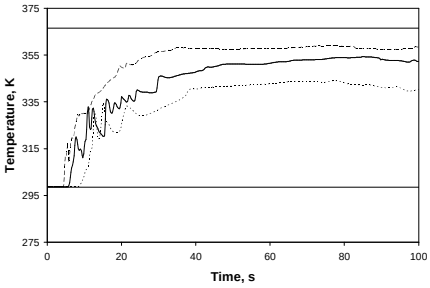

(b) Station C and 150^o from the injection point

Fig. 12 Comparison of the temperature profiles of varying injection flow rates (a) Station A and 150^o from the injection point and (b) Station C and 150^o from the injection point (- solid line – baseline case, long dashed line – double injection flow rate and short dashed line – half injection flow rate).

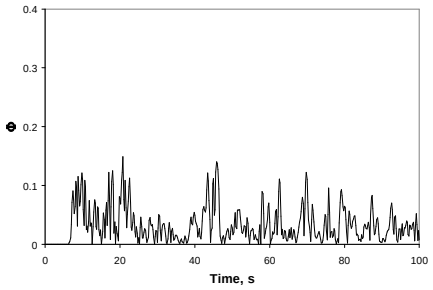

(a) Transient temperature fluctuations at A and 150^o

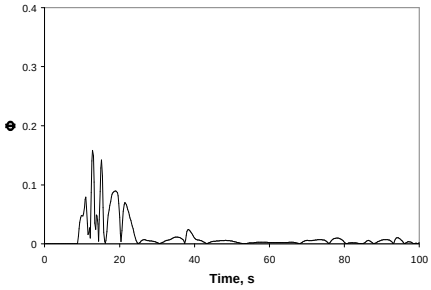

(b) Transient temperature fluctuations at C and 150^o

Fig. 13 Transient temperature fluctuations at Station A and Station C at 150^o from the injection point for the half injection flow rate case.

Transient normalized temperature fluctuations were studied for the varying injection flow rate cases by fitting a polynomial curves for the transient temperature profiles that were presented in Figure 12. Figures 13 and 14 show the normalized transient temperature fluctuations for the half and double injection flow cases. Figures 13(a) and 13(b) shows the temperature fluctuations at Station A and Station C measured at an angle of 150° from the injection point for the half injection flow rate case. For the half injection flow rate case, with the increase of the momentum ratio, sudden rise and fall of the temperature fluctuations were not observed at Station A 150°, but a continuously fluctuating magnitude ranging from 0 to 0.15 was observed. At Station C, the highest normalized temperature fluctuation was 0.15 in 0.6 seconds (i.e. 10.2 K in 0.6 seconds). After 20 seconds, the temperature fluctuations (0 to 0.02) at Station C 150° from the injection point where smaller when compared to the fluctuations at station A.

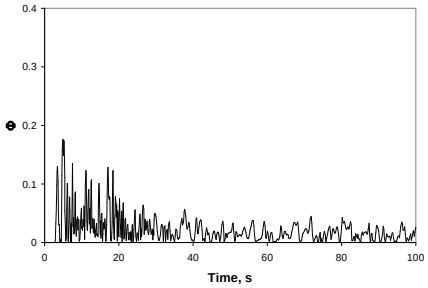

(a) Transient temperature fluctuations at A and 150^o

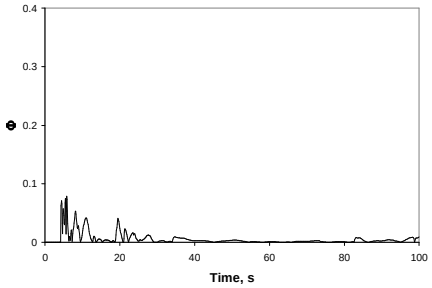

(b) Transient temperature fluctuations at C and 150^o

Fig. 14 Transient temperature fluctuations at Station A and Station C at 150^o from the injection point for the double injection flow rate case.

Figures 14(a) and 14(b) shows the temperature fluctuations at Station A and Station C measured at an angle of 150° from the injection point for the double injection flow rate case. At Station A, the highest normalized temperature fluctuation was 0.17 in 0.6 seconds (i.e. 11.6 K in 0.6 seconds) and at Station C, the highest normalized temperature fluctuation was 0.07 in 0.2 seconds (i.e. 5 K in 0.2 seconds). After 20 seconds, the temperature fluctuations magnitude (0 to 0.13) was higher at Station A 150° from the injection point when compared to the magnitude of the temperature fluctuations (0 to 0.002) at Station C 150° from the injection point. For the double injection flow rate case, with the decrease of the momentum ratio the hot injection flow is

more dominant and a higher temperatures where observed with reduced temperature fluctuations. Whereas with the half injection flow rates, due to the increase of the momentum ratio, higher temperature fluctuations where observed. Therefore, higher thermal stresses can be expected for the half injection flow rate case when compared to the other cases.

V. CONCLUSIONS

In this paper, numerical analysis were performed to study the transient thermal mixing induced by a sudden transverse injection of a fluid into a main flow of different temperatures using Reynolds stress turbulence model. The numerical model was validated with the available experimental results. To understand the mixing process, numerical simulations were performed with varying main and injection flow rates. Transient temperatures were plotted at various stations in the downstream and streamlines were presented on the injection plane for the baseline case. From the stream line plots, it was found that the hot injection flow was impinging on the walls of the main pipe very close to the injection line. After the flow impingement, the hot injection flow travelled in the upstream and downstream of the main feed water line parallel to the wall and a sharp rise in the wall temperatures was observed. Higher wall temperatures were observed at Stations near the injection point and lower temperatures were observed at Stations far from the injection point due to the mixing process. The thermal response was also slower at Stations far from the injection point. High temperature gradients were observed along the axial and circumferential directions close to the injection point and these temperature gradients results in the production of thermal stresses on the pipe walls.

After the initiation of the injection flow the hot injection flow trying to move in the upstream after the impingement and cold main flow trying to move downstream causes strong recirculation regions in the upstream of the injection point. This enhanced mixing in the upstream of the injection is due to the initial contact of the hot injection flow with the oncoming cold main flow. Flow entrainment into the hot injection jet was also observed close to the injection line. As the flow time increases, the cold main flow responded to the injection flow and relatively small recirculation regions were formed and confined to the region close to the injection point.

Parametric studies were also performed to study the temperature fluctuations by varying the main and injection flow rates. The temperature fluctuations were higher on the walls of the main pipe during the initial stage of the injection process. Higher temperature fluctuations were observed close to the injection point and the magnitude of the fluctuations were found to be decreasing along the downstream. The fluctuation magnitudes were almost constant during the steady injection process. As the difference between the momentum of the flows decreases, an increase in the temperature fluctuations were observed.

REFERENCES

[1] J. A. Schetz, Injection and mixing in turbulent flow, Progress in Astronautics and Aeronautics, American Institute of Aeronautics and Astronautics, New York, v. 68, (1980).

[2] Y. A. Hassan, J. H. Kim, A Navier-Stokes analysis of three-dimensional negatively buoyant jet injected into a hot cross flow, Nuclear Science and Engineering, v. 89, (1), (1985), January, 70-78.

[3] J. H. Kim, An analytical mixing model for buoyant jet injected into pipe flow, Journal of Heat Transfer, Transactions of ASME, v. 107, (3), (1985), August, 630-635.

[4] S. Moriya, N. Tanaka, N. Katana, , A. Wada, Effects of Reynolds number and Richardson number on thermal stratification in hot plenum, Nuclear Engineering and Design, v. 99, (1987), 441-451.

[5] W. Hafner, , L. Wolf, , Derivation of mixing parameters from the HDR-thermal mixing experiments, International Journal of Pressure Vessels and Piping, v. 33, (1), (1988), 41-57.

[6] R. Konduri, , Transient thermal mixing following sudden transverse injection of a fluid, M.S. Thesis, (1991), Tennessee Technological University, Cookeville, TN, U.S.A.

[7] F. Khodabaksh, R. Konduri, S.Munukutla, S. Idem, Transient thermal mixing following sudden transverse injection of a fluid, Journal of Thermophysics and Heat Transfer, v. 7, (4), (1993), October-December, 732-734.

[8] M. Wakamatsu, H. Nei, K. Hashiguchi, Attenuation of temperature fluctuations in thermal striping, Journal of Nuclear Science and Technology, v. 32, (1995), 752-762.

[9] H.G. Lele, S.K. Gupta, H.S. Kushwaha, V. Venkat Raj, Modelling of thermal and flow stratification for reactor pressure vessel pressurized thermal shock, Nuclear Engineering and Design, v. 212, (2002), 75-84.

[10] M. Hirota, H. Asano, H. Nakayama, T. Asano, , S. Hirayama, Three dimensional structure of turbulent flow in mixing T- junction, JSME International Journal Series B, v. 49, (4), (2006), 1070-1077.

[11] N. Fukushima, K. Fukagata, N. Kasagi, H. Noguchi, K. Tanimoto, Numerical and experimental study on turbulent thermal mixing in a T-junction flow, The 6th ASME – JSME Thermal Engineering Joint Conference, (2003) March 16-20.

[12] K. J. Metzner, U. Wilke, European THERFAT project – thermal fatigue evaluation of piping system "Tee" - connections, Nuclear Engineering and Design, v. 235, (2005), 473-484.

[13] S. Chapuliot, , C. Gourdin, , T. Payen, , J. P. Magnaud, A. Monavon, Hydro-thermal-mechanical analysis of thermal fatigue in a mixing tee, Nuclear Engineering and Design, v. 235, (5), (2005), February, 575-596.

[14] L. W. Hu, M. S. Kazimi, LES benchmark study of high cycle temperature fluctuations caused by thermal striping in a mixing tee, International Journal of Heat and Fluid Flow, v.27, (1), (2006), February, 54-64.

[15] Fluent 6.3. Documentation, Fluent, Inc., Lebanon, NH, 2003.

[16] S. B. Pope, *Turbulent Flows*, Cambridge University Press, New York, Chapter 11, (2000)